1 **Surface phenotyping and quantitative proteomics reveal differentially enriched proteins of**

2 **brain-derived extracellular vesicles in Parkinson's disease**

3

4 Tanina Arab [1], Yiyao Huang [1], Rajini Nagaraj [2], Evan Gizzie [2], Javier Redding-Ochoa [3,4], Juan C.

5 Troncoso [3,4], Olga Pletnikova[4,5], Tatiana Boronina[6], Robert N. Cole[6], Vasiliki Mahairaki [7,8], David

6 A. Routenberg [2], Kenneth W. Witwer [1,3,8,]*

7

8 [1] Department of Molecular and Comparative Pathobiology, Johns Hopkins University School of

9 Medicine, Baltimore, MD, USA

10 [2] Meso Scale Diagnostics, LLC, Rockville, MD, USA

11 [3] Department of Neurology, Johns Hopkins University School of Medicine, Baltimore, MD, USA

12 [4] Department of Pathology, Johns Hopkins University School of Medicine, Baltimore, MD, USA

13 [5] Department of Pathology and Anatomical Sciences, Jacobs School of Medicine and Biomedical

14 Sciences, University at Buffalo, Buffalo, NY, USA

15 [6] Department of Biological Chemistry, Johns Hopkins University School of Medicine, Baltimore,

16 MD, USA

17 [7] Department of Genetics, Johns Hopkins University School of Medicine, Baltimore, MD, USA

18 [8] The Richman Family Precision Medicine Center of Excellence in Alzheimer's Disease, Johns

19 Hopkins University School of Medicine, Baltimore, MD, US

20 *Corresponding author. Email: kwitwer1@jhu.edu

21 **ABSTRACT**

22 Extracellular vesicles (EVs) are produced by all cell types and are found in all tissues and

23 biofluids. EV proteins, nucleic acids, and lipids are a "nano-snapshot" of the parent cell that may

24 be used for novel diagnostics of various diseases, including neurodegenerative disorders.

25 Currently, diagnosis of the most common neurodegenerative movement disorder, Parkinson's

26 disease (PD), relies on manifestations of late-stage progression, which may furthermore

27 associate with other neurodegenerative diseases such as progressive supranuclear palsy (PSP).

28 Here, we profiled surface markers and other protein contents of brain-derived extracellular

29 vesicles (bd-EVs) from PD (n= 24), PSP (n=25) and control (n=24). bdEVs displayed tetraspanins

30 and certain microglia, astrocyte, and neuron markers, while quantitative proteomics revealed

31 enrichment of several proteins in PD vs. control and/or PSP, including clathrin heavy chain 1 and

32 14-3-3 protein gamma. This characterization of EVs in the source tissue provides insights into

33 local dynamics as well as biomarker candidates for investigation in peripheral fluids.

34

35 **Keywords:** Parkinson's disease, microglia, astrocytes, neurons, extracellular vesicles,

36 ectosomes, exosomes, biomarkers, proteomics, progressive supranuclear palsy

INTRODUCTION

Parkinson's disease (PD) is the most common neurodegenerative movement disorder, affecting approximately 1% of individuals over 65 years of age (de Lau & Breteler, 2006). PD is characterized by loss of pigmented neurons in the locus ceruleus and substantia nigra (Fearnley & Lees, 1991) and neuronal abnormal aggregation of alpha-synuclein (α-syn) (e.g., Lewy bodies (LBs) and Lewy neurites) (Hijaz & Volpicelli-Daley, 2020; J. Y. Li et al., 2008). Since neuronal loss in the brain is irreversible, drugs that delay or prevent neurodegeneration are more effective if prescribed at early stages of pathology. However, PD diagnosis may not occur until late, and PD can also be confused with other parkinsonian disorders, such as progressive supranuclear palsy (PSP) (Hughes et al., 2002; Joutsa et al., 2014). Therefore, reliable, specific, and easily accessed biomarkers of PD are urgently needed (Mark Frasier and Un Jung Kang, 2014).

Extracellular vesicles (EVs) already serve as biomarkers of, e.g., prostate cancer (McKiernan et al., 2020) and have elicited growing interest in the neurodegenerative disease field (Cao et al., 2019; Dutta et al., 2021; Gámez-Valero et al., 2019; Trotta et al., 2018; Wu et al., 2017). EVs are lipid bilayer-delimited nanoparticles released by various cells (Cocozza et al., 2020; van Niel et al., 2018; Yates et al., 2022), including those in the central nervous system (CNS) (Coleman & Hill, 2015; Krämer-Albers & Hill, 2016). EVs remove cellular toxins, participate in cell signaling, transfer molecular cargo, including nucleic acids and proteins, and serve as trophic factors (Maas et al., 2017; Russell et al., 2019; Yáñez-Mó et al., 2015).

In PD, peripheral biofluid EVs have been suggested as potential biomarkers, for example, for the purpose of stratifying cohorts (Alvarez-Erviti et al., 2011; Emmanouilidou et al., 2010; Stuendl et al., 2021), with the assumption that CNS EVs can escape to the periphery or that peripheral EVs otherwise reflect the state of the brain. Various PD-related proteins, such as alpha-synuclein (α-syn) (Emmanouilidou et al., 2010), LRRK2, and DJ-1 (Hong et al., 2010) are carried by EVs and, in some cases, enriched during lysosomal pathway failure (Alvarez-Erviti et al., 2011; Danzer et al., 2012). EVs have also been investigated in mitochondrial or oxidative stress and calcium

3

63   dysfunction (Eitan et al., 2016; Fan et al., 2019). Although peripheral biofluid EV molecular profiles

64   have been examined at the RNA and protein levels (Dutta et al., 2021; Jiang et al., 2021; Shi et

65   al., 2014), how these findings compare with EVs present in the brain remains unclear. Brain-

66   derived EVs (bdEVs) can be separated by gentle tissue digestion in a reproducible manner

67   (Huang et al., 2020; Vella et al., 2017). Here, we separated and profiled bdEVs from PD, PSP,

68   and control tissues. Our goals were to understand whether and how pathological conditions are

69   reflected in EV molecular cargo and to identify molecules for capture and profiling of peripheral

70   bdEVs.

71   **MATERIALS AND METHODS**

72   *See Table 1 for manufacturers, catalog numbers, and other information.*

73   **Tissue collection and preparation**

74   Human postmortem brain tissue samples were archived at -80°C by the Brain Resource Center

75   (Department of Pathology, Johns Hopkins University School of Medicine) following brain autopsy

76   with full neuropathological examination. For tissue dissection, neuroanatomical identification of

77   the inferior parietal gyri was performed on coronal sections from 73 individuals (PD: n= 24; PSP:

78   n=25; Control: n=24). The selected brain tissues were placed in a -20°C freezer for 15 minutes.

79   Sterile 4-mm-diameter tissue punches were then used to extract samples from the inferior parietal

80   cortex at the level of supramarginal and angular gyri. Samples were again stored at −80°C prior

81   to bdEV separation. Several additional samples were obtained from the brain bank for the purpose

82   of training and tool comparison. To minimize the influence of batch effects and operator bias,

83   samples were de-identified by an individual not involved in the study and assigned to processing

84   batches with an equal or approximately equal number of samples from each clinical group. De-

85   identified samples were processed in these batches. Table 2 summarizes the cohort information,

86   which was made available to investigators only after all data were obtained and archived.

87   **Brain-derived extracellular vesicle separation**

88   EVs were separated from tissue as previously described (Huang et al., 2020). The frozen tissue

89   was weighed, sliced on dry ice, and gently digested using collagenase type 3 enzyme in

90   Hibernate-E solution for 20 min at 37°. 1X PhosSTOP and Complete Protease Inhibitor solution

91   (PI/PS) were added to stop the enzymatic reaction. Differential centrifugation was performed at

92   4°C. First, the dissociated tissue was centrifuged at 300 × g for 10 min. A small portion of each

93   pellet ("brain homogenate with collagenase," BHC) was stored at −80°C for later protein

94   extraction. Supernatant was pipetted off using a 10 mL serological pipette, transferred to a fresh

95   tube, and centrifuged at 2000 × g for 15 min. The "2K" pellets were snap-frozen and saved at -

96   80°C. The supernatant was further depleted of debris and large bodies through a gentle 0.22-μm

97   filtration at a slow flow rate of 5 mL/min. Filtered material was centrifuged at 10,000 x g for 30 min

98   using swinging-bucket rotor TH-641 (Thermo Scientific, k-factor 114, acceleration and

99   deceleration settings of 9). Pellets ("10K") were resuspended in 150 μl PBS containing 1X PI/PS

100 by pipetting up and down ten times, vortexing 30 seconds, and incubating on ice 20 minutes,

101 followed by a repeat of the pipetting and vortexing steps. Thusly resuspended 10K bdEVs were

102 aliquoted and stored at -80°C. Supernatants were transferred into 100 kilodaltons (kDa) molecular

103 weight cut-off (MWCO) protein concentrators (Thermo Fisher, 88524), and volumes were reduced

104 from 5 mL to 0.5 mL. Retentate was then applied to the top of qEV Original size exclusion

105 chromatography (SEC) columns (Izon Science, Cambridge, MA) that were pre-rinsed with 15 ml

106 PBS. 0.5 mL fractions were collected by elution with PBS, using Izon automated fraction collectors

107 (AFCs; Izon Science, Cambridge, MA). Fractions 1-6 (≈ 2.8 mL) were considered the void volume;

108 fractions 7-10 were pooled as EV-enriched fractions; and fractions 11-14 were pooled as protein-

109 enriched fractions. EV-enriched fractions were transferred to polypropylene UC tubes and

110 centrifuged at 100,000 × g for 70 min, using the TH-641 swinging-bucket rotor as described

111 above. Supernatant was poured off, and UC tubes were stood upright and inverted on a piece of

112 tissue to remove residual buffer. Pellets ("100K") were resuspended following the same procedure

113 described above, but by adding 120 μl PBS (1X PI/PS) to each tube. Aliquots were stored at -

114 80°C.

115 **Nano-flow cytometry measurement (NFCM)**

116 Particle concentration and size profiles were assessed by nano-flow (Flow NanoAnalyzer,

117 NanoFCM, Nottingham, England) using side scatter, as described previously (Arab et al., 2021;

118 Huang et al., 2020). Instrument calibrations for concentration and size distribution were done

119 using 200-nm polystyrene beads and a silica nanosphere mixture (68-155 S16 M-EXO),

120 respectively. After calibration, settings remained unchanged during sample evaluation. For each

121 sample, 2 μl of bdEV resuspension was used. Serial dilutions were performed as needed to fall

122   within the manufacturer's recommended particle count range (Arab et al., 2021), and events were

123   recorded for 1 min. Flow rate and side-scatter intensity were converted into particle concentration

124   and size distribution using calibration curves.

Transmission electron microscopy (TEM)

126   12 of 73 samples were randomly chosen and imaged by TEM as previously described (Arab et

127   al., 2021). Briefly, 10 µl of each sample was freshly thawed and adsorbed to glow-discharged

128   carbon-coated 400 mesh copper grids by flotation for 2 min. Three consecutive drops of 1× Tris-

129   buffered saline were prepared on Parafilm. Grids were washed by moving from one drop to

130   another, with a flotation time of 1 min on each drop. The rinsed grids were then negatively stained

131   with 1% uranyl acetate (UAT) with tylose (1% UAT in deionized water (dIH2O), double-filtered

132   through a 0.22-µm filter). Grids were blotted, then excess UAT was aspirated, leaving a thin layer

133   of stain. Grids were imaged on a Hitachi 7600 TEM operating at 80 kV with an XR80 charge-

134   coupled device (8 megapixels, AMT Imaging, Woburn, MA, USA).

Western blot (WB)

136   BH, BHC, 2K, 10K, and EV and protein SEC fractions were lysed in 1× radioimmunoprecipitation

137   assay buffer (RIPA) supplemented with protease inhibitor cocktail. A total of 20 µL of lysates were

138   resolved using a 4% to 15% Criterion TGX Stain-Free Precast gel, then transferred onto an

139   Immuno-Blot PVDF membrane. Antibodies to CD81, CD63, and CD9 were used to detect EV

140   membrane markers, and anti-GM130 antibody was used to detect Golgi intracellular

141   contamination. Antibodies were diluted in PBS-T containing 5% blotting-grade blocker (Bio-Rad,

142   #1706404). Membranes were incubated overnight (≈16 h). After several washes in PBS-T, rabbit

143   anti-mouse IgGk BP-HRP and mouse anti-rabbit IgGk BP-HRP secondary antibodies were diluted

144   in blocking buffer, and membranes were incubated for 1 h at room temperature (RT). Pierce™

145   ECL Western Blotting Substrate (Thermo Fisher, 32106) was applied, and blots were visualized

146   using a Thermo Fisher iBright 1500 imaging system.

Single-particle interferometric reflectance imaging sensor (SP-IRIS)

148   EVs were phenotyped with EV-TETRA-C ExoView Tetraspanin kits and an ExoView TMR100

149   scanner (NanoView Biosciences, Boston, MA) according to the manufacturer's instructions and

150   as described previously (Arab et al., 2021). Concentrations as measured by NFCM, were adjusted

151   such that around 1e9 particles from each sample were mixed 1:1 with ExoView incubation buffer

152   (IB). 35µl of this mixture was placed onto the chip and incubated at RT for 16h (no shaking). Chips

153   were washed with IB and incubated 1h at RT with a fluorescently-labeled antibody cocktail of anti-

154   human CD81 (JS-81, CF555), CD63 (H5C6, CF647), and CD9 (HI9a, CF488A) at dilutions of

155   1:1200 (v:v) in a 1:1 (v:v) mixture of IB and blocking buffer. All chips were scanned and imaged

156   with the ExoView scanner using both SP-IRIS Single Particle Interferometric Reflectance Imaging

157   Sensor and fluorescence detection. Data were analyzed using NanoViewer 2.8.10 Software.

158   **Multiplexed ELISA**

159   Prototype S-PLEX® ultrasensitive assays (Meso Scale Diagnostics, Rockville, MD) were used for

160   intact EVs. Five multiplexed assay panels were assembled in this fashion. According to the

161   manufacturer's recommendations, samples were diluted up to 30-fold in "diluent 52," added to the

162   plates, and incubated at RT with continuous shaking. Panel 1, comprising antibodies targeting

163   relatively abundant surface markers, was incubated for 1 hour, while the remaining panels,

164   targeting lower-abundance markers, were incubated for 4 hours to improve sensitivity. EVs

165   captured by each antibody were detected using MSD's S-PLEX® ultrasensitive assay methods

166   with a cocktail of detection antibodies targeting CD63, CD81, and CD9. Assay plates were read

167   with MSD GOLD™ Read buffer B on an MSD® SECTOR instrument. bdEVs from the 73 subjects,

168   as well as additional positive and negative controls, were assayed with each panel.

169   **Relative quantification proteomics**

170   *Sample preparation, protein digest, peptide TMT labeling*. Proteins were extracted from 20 µl of

171   resuspended bdEVs separated from the inferior parietal region of Parkinson's (n=5), Progressive

172   Supranuclear Palsy (n=5), and matched controls samples (n=5) using RIPA buffer (Cell Signaling

173   Technology). Disulfide bonds were reduced using 50 mM dithiothreitol (Sigma, D0632) and

8

174 cysteine residues were alkylated with iodoacetamide (Sigma, I1149) as previously described

175 (Arab et al., 2019). Resulting protein lysates were precipitated with trichloroacetic acid (TCA)

176 (Sigma, T0699). Briefly, samples were supplemented with 10% of TCA in acetone solution in a

177 ratio of (1:8, V/V). After precipitation, pellets were resuspended in 50 mM ammonium bicarbonate

178 containing 10% acetonitrile, sonicated for 10 min, and pH was adjusted to 7.8–8.0 using Tris

179 Hydrochloride, pH 8.0. Proteins were digested with 12 ng/mL Trypsin/Lys-C (Thermo Fisher

180 Scientific # A41007) overnight at 37 °C. Digested peptides were labeled with 16-plex TMT isobaric

181 mass tag reagents (Thermo Fisher Scientific) according to the manufacturer's instructions.

182 Labeled peptides were loaded onto a Pierce detergent removal column (Thermo Fisher # 87779)

183 and eluted in 300 µL of 8% Triethylammonium bicarbonate, 0.1% Trifluoroacetic acid, and 92%

184 water. Prior to mass spectrometry analysis, peptides were desalted on u-HLB Oasis plates

185 (Waters), eluted in a buffer containing 60% acetonitrile and 0.1%TFA, and dried by vacuum

186 centrifugation.

187 *Liquid chromatography separation and tandem mass spectrometry (LC-MS/MS).* Desalted

188 peptides were reconstituted in 40 µL solution buffer containing 2% ACN and 0.1% FA

189 andanalyzed by nano-LC tandem mass spectrometry (LC-MS/MS) using a Orbitrap-Lumos-

190 Fusion mass spectrometer (Thermo Fisher Scientific) interfaced with a EasyLC1200 series

191 equipped with ProntoSIL-120-5-C18 H BISCHOFF reverse phase column (75 µm × 150 mm, 3

192 µm). Peptides were separated using a 2%–90% acetonitrile gradient in 0.1% FA over 78 min at a

193 flow rate of 300 nL/min. Eluting peptides were electrosprayed at 2.4 kV into an Orbitrap-Lumos-

194 Fusion mass spectrometer through a 1 µm emitter tip (New Objective). Survey scans (MS1) of

195 peptides between 375 and 1600 m/z were acquired at 120,000 FWHM resolution (at 200 m/z)

196 and 4e5 automatic gain control (AGC). By data-dependent acquisition, the 15 most intense ions

197 were individually isolated with 0.7 m/z window and fragmented (MS/MS) using a 38 higher-energy

198 collisional dissociation (HCD) activation energy and 15 sec dynamic exclusion. Fragment ions

199 were analyzed at a resolution of 60,000 FWHM and 5e4 AGC.

200   *Raw data processing and analysis.* All the tandem MS/MS spectra (signal/noise >2) were

201   processed by Proteome Discoverer (v2.4 Thermo Fisher Scientific). MS/MS spectra were

202   searched with Mascot v.2.6.2 (Matrix Science, London, UK), and proteins were identified by

203   searching against the 2021_204_H_sapiens database. Trypsin specificity was used for the

204   digestion, with up to two missed cleavages. Methionine oxidation and deamidation were selected

205   as the variable modifications. Carbamidomethylation of cysteines and TMT-label modifications of

206   N-termini and lysine were set as fixed modifications. Based on a concatenated decoy database

207   search, Proteome Discoverer-Percolator was used to validate identified peptides with a

208   confidence threshold of 1%. Proteome Discoverer used TMT reporter ions from peptide-matched

209   spectrum (PSM) of unique Rank 1 unmodified peptides with reporter signal/noise >5 and an

210   isolation interference <25 to calculate and normalize protein ratios

211 based on the normalized median ratio of all spectra of tagged peptides from the same protein

212 (Herbrich et al., 2013). Gene ontology terms were determined using PANTHER V17.0 software

213 **Statistical analysis and data and methods availability**

214 Differences in total EV particle concentrations and in surface markers expression were assessed

215 by Kruskal-Wallis ANOVA test in GraphPad Prism 9 (GraphPad Software Inc., La Jolla, CA).

216 Results were considered significant if p-value < 0.05. For labeled proteins, significant differential

217 abundance was defined as Log 2-fold-change = 0.32 and p-value <0.05. p-values and adjusted

218 p-values (Benjamini-Hochberg method) were calculated using a non-nested ANOVA test per

219 Proteome Discoverer 2.4 recommendations.

220 All relevant experimental details were submitted to the EV-TRACK knowledgebase (EV-TRACK

221 ID: EV220312) (van Deun et al., 2017). Proteomic data are available upon request.

RESULTS

bdEV separation and characterization

bdEVs were separated from brain tissue of a selected cohort of Parkinson's, PSP, and control donors (PD: n= 24; PSP: n=25; Control: n=24) in compliance with the international consensus guidelines for studies of EVs (MISEV2018) (Théry et al., 2019). Characterization of specific markers included Western blot and SP-IRIS for several samples with greater availability, and, for more precious cohort samples, proteomics and multiplexed ELISA. For selected samples, Western blot (WB) showed low levels of CD63 but abundant CD9 and CD81; Golgi marker GM130 was relatively depleted (Fig. 2a). Similarly, SP-IRIS confirmed that bdEVs were positive for the tetraspanins CD81, CD63, and CD9, along with cytosolic EV marker Syntenin (Fig 2b). Fluorescence signals for CD63 and Syntenin were similar across tetraspanin capture spots, whereas fluorescence for CD9 and CD81 varied based with capture antibody (Sup Fig. 1 c-g).

For all cohort samples, particle counts and size distribution per 100 mg of tissue were measured using NFCM. There were no significant differences in particle counts (Fig. 2c), size distribution profiles (Fig. 2d), or mean size (Fig. supp 1b) between PD, PSP, and control groups. Diameter distribution profiles for each group displayed the same pattern, with a peak around 65 nm. TEM images of randomly selected samples across control, PD, and PSP groups showed particles with expected EV morphology and size (Fig. 2c). Consistent with NFCM, there were no differences in size and yield by group (Fig. 2c, supp Fig. 1a). Additional characterization by mass spectrometry and ELISA surface phenotyping is presented below.

bdEV, tetraspanin, and cell marker phenotyping suggest disease-associated differences

To assess the relative contribution of each brain cell type to total bdEVs, multiplexed ELISAs were used to assay 36 proteins, including markers of one or more specific cell types: microglia, neurons, astrocytes, and endothelial cells (Fig. 3a).

246 **_Tetraspanins._** CD63 signal was significantly greater in PD compared with the control group. CD81 and CD9 signals were significantly higher for PD and PSP than controls (Fig. 3b), but there were no differences between the disease groups. Several cellular origin surface markers were increased in bdEVs from PD patients compared with control (Fig. 3).

250 **_Microglial markers._** Transmembrane protein 119 (TMEM119), C-X3-C motif chemokine receptor 1 (CX3CR1), translocator protein (TSPO), CD33, and CD36 were significantly more abundant in PD and PSP compared with control, but the difference between PD and PSP was not statistically significant (Fig. 3c). Stabillin-1 differentiated PSP from control and glycoprotein nonmetastatic melanoma protein B (GPNMB) was different between PD from control (Supp Fig. 3a; note that some values are negative due to background subtraction). CD64, major histocompatibility complex class II (HLA-DR/DP/DQ), CD163, CD68, and CD32b showed no significant difference between groups (Supp Fig. 2a). Triggering receptor expressed on myeloid cells 2 (TREM2), CD11b, CD18, and MER proto-oncogene, tyrosine kinase (MERTK) were below the limit of detection (data not shown) ITGB5.

260 **_Neuronal markers._** CD24, nerve growth factor receptor (CD271), and neuronal cell adhesion molecules NRCAM and NCAM were significantly different for disease groups compared with controls, but PD did not differ from PSP. Thy-1 cell surface antigen (CD90/Thy1) and CD166 differed between PD and control but not between PSP and control. Only low levels of signal for L1 cell adhesion molecule (L1CAM) were detected, with no significant differences between groups (Fig. 3d).

266 **_Astrocytic markers._** Ganglioside G2 (GD2) and CD44 were detected abundantly compared with ganglioside GD1a (GD1a) and gap junction alpha-1 protein (GJA1, Fig. 3e). These markers show significant differences between the pathological groups compared with control.

269 ***Endothelial markers.*** Platelet and endothelial cell adhesion molecule 1 (CD31) differed in the

270 pathological groups compared with the control group, whereas melanoma cell adhesion molecule

271 (CD146) differentiated PD, but not PSP, from control (Fig. 3f).

272 ***Non-tetraspanin proteins found in multiple cell types.*** Fucosyl transferase 4 (CD15) and

273 CD40, found on both microglia and astrocytes, distinguished both disease groups from control

274 (Fig. 3g), whereas integrin subunit beta 5 (ITGB5) showed no significant differences between

275 tested groups (Supp Fig. 2b). CD38 (cluster of differentiation 38), also known as cyclic ADP ribose

276 hydrolase, and Fc receptor-like 4 (CD307d), both of which are found on microglia, astrocytes, and

277 neurons, differentiated PD from PSP and pathological groups from the control group, respectively

278 (Fig. 3h). CD307d showed values close to background for the majority of tested samples (Supp

279 Fig. 2 c). Integrin subunit beta 1 (CD29), a marker detected in all cells, distinguished both disease

280 groups from control (Fig. 3 i).

281 **Differentially expressed proteins in brain-derived EVs as revealed by quantitative**
282 **proteomics**

283 Relative quantitative mass spectrometry was performed for bdEVs from five individuals in each

284 group (PD, PSP, and control). A total of 1369 proteins were detected in at least one sample.

285 Amongst these proteins, the gene ontology (GO) term "transport" was the most represented

286 (Supp Fig. 3a). 306 master proteins were successfully tagged for quantitative comparison. After

287 removing duplicates, per calculated ratios PD vs. control, PD vs. PSP, and PSP vs. control, 26

288 proteins were identified as significantly differentially abundant (Fig. 4a, Table 3). In this list, there

289 are 17 proteins less abundant by Log 2-fold-change (Log_2 fc) less than or equal to - 0.32 and p-

290 value <0.05, and 7 proteins more abundant by Log_2 fc greater than or equal to 0.32 and p-value

291 <0.05 (Supp Fig. 3b-d). Ankyrin-1 (ANK1) and stomatin (STOM) were more abundant in PSP vs.

292 control and less abundant in PD vs. PSP.

293 Plasma membrane calcium-transporting ATPase 2 (ATP2B2), guanine nucleotide-binding protein

294 G subunit beta-2 (GNB2), and guanine nucleotide-binding protein G subunit gamma-3 (GNG3)

13

295   differed only between PD vs. control, with lower abundance in PD (Fig. 4b). Five proteins differed

296   only between PD and PSP (Fig. 4c). Clathrin heavy chain 1 (CLTC), F-actin-capping protein

297   subunit alpha-1 (CAPZA1), ADP-ribosylation factor 5 (ARF5), synaptic vesicle glycoprotein 2A

298   (SV2A) were less abundant in PD, whereas cathepsin D (CTSD) was more abundant.

299   Comparison between PSP and control returned three unique proteins more abundant in PSP;

300   namely excitatory amino acid transporter 1 (SLC1A3), erythrocyte membrane protein band 4.2

301   (EPB42), and solute carrier family 2 (SLC2A1) (Fig. 4d).

302   Eleven proteins overlapped between PD vs. control and PD vs. PSP (Fig. 4e). Calcium-

303   transporting ATPase 1 (ATP2B1), glial fibrillary acidic protein (GFAP), 14-3-3 GAMMA (YWHAG),

304   sodium/calcium exchanger 2 (SLC8A2), brevican core protein (BCAN), ribosomal protein S9

305   (RPS9), ribosomal protein S18 (RPS18), ribosomal protein L15 (RPL15), actin-related protein 2

306   (ACTR2) were less abundant in PD, whereas Ras-related protein Rap-1b (Rap1b) and hyaluronan

307   and proteoglycan link protein 2 (HAPLN2) were more abundant in PD. Two proteins overlapped

308   between PD vs. control and PSP vs. control (Fig. 4f), and two proteins overlapped between PD

309   vs. PSP and PSP vs. control (Fig. 4g). Although our mass spectrometry protocol was not directed

310   towards membrane proteins, several membrane markers measured by ELISA were also detected

311   by mass spectrometry (Table 4), including astrocyte marker CD44 and neuronal marker NCAM1.

312   EV marker CD81 was detected but not TMT labeled.

313   **Presence of classical EV markers and Parkinson's disease-related proteins in brain-**
314   **derived extracellular vesicles from Parkinson's subjects**

315   Next, we compared our proteomic data set to the ExoCarta "Top 100" list of putative EV-

316   associated proteins. 47 proteins were present in our samples, with 37 successfully labeled with

317   TMT tags and 10 not labeled (Table 5). Some have already been listed as distinguishing bdEV

318   from the tested groups, e.g., YWHAG, STOM, GNB2, RAP1B, and CLTC. More EV markers were

319   identified but without statistically significant differences between tested groups, e.g., CD81,

320   flotillin-1 (Flot-1), RAB proteins (RAB1A, RAB5c), annexins (ANXA1, ANXA11, ANXA2, ANXA4,

14

321   ANXA5, ANXA6), enolase-1 (Eno1), and 14-3-3 proteins (YWHAE, YWHAH, YWHAQ, YWHAZ).

322   In addition, flotillin-2 (Flot-2) and syntenin-1 EV markers are present in our data set but not in the

323   top-100 ExoCarta list.

324   We followed a similar approach and compared a list of 1952 known PD genes downloaded from

325   DisGeNET with our data set (Supp Fig. 4a). We found 80 to overlap with identified proteins,

326   including 58 that were successfully labeled. Interestingly, several genes overlap with differentially

327   abundant proteins listed above, including YWHAG, RAP1B, HAPLN2, ANK1, and CTSD.

328   Although not all of the 58 labeled proteins were selected after the applied thresholds (Log 2-fold-

329   change of 0.32 and p-value <0.05), abundances ratios in PD vs. Control and PD vs. PSP were

330   calculated (Supp Fig. 4b). Among listed proteins, SOD1 and SLC16A1 had ratios > 1 in PD vs.

331   Control and PD vs. PSP, suggesting these proteins are more abundant in PD bdEVs. On the other

332   hand, alpha-synuclein (SNCA) had ratios < 1 in PD vs. Control and PD vs. PSP, suggesting lower

333   abundance in PD, whereas Parkinson's disease protein 7 (PARK7) returned divergent ratios of

334   0.87 and 1.103 in PD vs. Control and PD vs. PSP respectively, suggesting that PARK7 is less

335   abundant in PD vs. control but more abundant in PD vs. PSP.

336   **DISCUSSION**

337   **Summary of results**

338   EV biomarkers of tissue pathology may be most valuable if they migrate into and can be found in

339   accessible biofluids. To know what to look for in the periphery, we must thus know what is present

340   in the cell and tissue of origin. Here, we report proteomic profiling of bdEVs purified from PD,

341   PSP, and control brain tissues, finding several markers that differentiate groups. To the best of

342   our knowledge, SLC8A2 and HAPLN2 differences are described for the first time as distinguishing

343   bdEVs in PD. Some of these proteins, especially those implicated in endosomal pathway

344   regulation, may serve not only as possible biomarkers but also as indicators of mechanisms in

345   PD. Additionally, surface phenotyping of intact bdEVs showed the presence of selected neuronal,

346   microglial, astrocytic, and endothelial markers that could be used in future to separate putative

15

347   bdEVs from peripheral samples. We would now like to highlight several proteins of interest that

348   we evaluated.

349   ***SLC8A2***

350   SLC8A2 (NCX2) is a brain-specific Na+/Ca2+ exchanger (Jeon et al., 2003)(Calabrese et al.,

351   2022). Mitochondrial SLC8A2 regulates calcium exchange in dopaminergic neurons, preventing

352   calcium-dependent neurodegeneration (Gandhi et al., 2009; Wood-Kaczmar et al., 2008, 2013).

353   NCX2 was reported to play a neuroprotective role in the ischemic model of the adult mouse brain

354   (Jeon et al., 2008). Examination of NCX2 in synaptosomes of human brain specimens of

355   Alzheimer's disease revealed an increase of NCX2 in positive terminals and a colocalization with

356   amyloid b in synaptic terminals (Sokolow et al., 2011). Because of its brain tissue specificity,

357   localization at the cell membrane, presence in EVs, and potential involvement in PD, NCX2 is a

358   promising candidate for more in-depth validation of mitochondrial dysfunctions seen in PD at the

359   EV level.

360   ***HAPLN2***

361   HAPLN2, also known as brain-derived link protein1 (Bral1), was more abundant in bdEVs in PD

362   as previously reported in tissue (Liu et al., 2015). HAPLN2 is thought to be a secreted protein

363   and to play a role in extracellular matrix formation and maintenance and neuronal conductivity

364   (Bekku et al., 2009, 2010). Elevated HAPLN2 was linked to alpha-synuclein aggregation in an

365   animal model of PD (Wang et al., 2016). More recently, HAPLN2 was reported (Teeple et al.,

366   2021) to have significantly greater expression across oligodendrocyte clusters in PD vs.

367   controls. Our results suggest the possibility that HAPLN2 overexpression is also reflected in EV

368   association. We speculate that this protein might be involved in spread of PD pathology.

369   ***TMEM119***

370   Microglially-enriched TMEM119 was elevated in PD and PSP in our assays. Although TMEM119

371   has been reported as specific for microglia, at least in the CNS (Bennett et al., 2016; Q. Li & Barres,

372   2018; Zhang et al., 2014), its levels may fluctuate during neuroinflammation (Bennett et al., 2016),

373   and TMEM119-positive cells declined in a PD mouse model (George et al., 2019). We detected

374   TMEM119 in some samples but not in others. Further studies are thus needed to determine if

375   TMEM119 will be a valuable candidate for obtaining EVs from biofluids to assess the health of

376   CNS microglia. Given the differing directions of regulation in neuroinflammation and PD, it may

377   also be necessary to evaluate TMEM119 in patients at different stages and with different co-

378   morbidities to assess its value in a diagnostic tool.

379   ***L1CAM***

380   L1CAM affinity strategies have been used to obtain peripheral EVs of putative neuronal origin for

381   biomarker discoveries, including in PD (Dutta et al., 2021; Jiang et al., 2021; Shi et al., 2014).

382   However, neuronal specificity (Gutwein et al., 2003, 2005) and EV association (Norman et al.,

383   2021) have both been questioned (Gomes & Witwer, 2022). Here, even in bdEVs, we detected only

384   very low signals for L1CAM compared with other neuronally enriched markers, such as NCAM,

385   NRCAM, and CD90 (Fig 3d). Like L1CAM, these proteins are also found on non-neuronal cells

386   and outside the CNS.

387   In conclusion, multiple apparent PD markers were identified in this study, offering opportunities

388   for follow-up. A strength of our study was the use of complementary profiling approaches. While

389   the relatively unbiased proteomics approach was not specifically focused on membrane proteins

390   (Hu et al., 2018), it was complemented by a targeted multiplexed ELISA approach to measure

391   brain cell type-specific markers including membrane-associated proteins. Despite a relatively

392   modest group size, significant differences were detected across categories. These differences

393   are thus even more likely to be detected in larger validation cohorts. In sum, our study identified

394   several brain cell type-specific markers on the surface of bdEVs that may be exploited for

395   detection in the periphery, as well as markers that distinguish disease and control groups.

396

BIBLIOGRAPHY

Alvarez-Erviti, L., Seow, Y., Schapira, A. H., Gardiner, C., Sargent, I. L., Wood, M. J. A., & Cooper, J. M. (2011). Lysosomal dysfunction increases exosome-mediated alpha-synuclein release and transmission. *Neurobiology of Disease*, *42*(3), 360–367. https://doi.org/10.1016/j.nbd.2011.01.029

Arab, T., Mallick, E. R., Huang, Y., Dong, L., Liao, Z., Zhao, Z., Gololobova, O., Smith, B., Haughey, N. J., Pienta, K. J., Slusher, B. S., Tarwater, P. M., Tosar, J. P., Zivkovic, A. M., Vreeland, W. N., Paulaitis, M. E., & Witwer, K. W. (2021). Characterization of extracellular vesicles and synthetic nanoparticles with four orthogonal single-particle analysis platforms. *Journal of Extracellular Vesicles*, *10*(6). https://doi.org/10.1002/jev2.12079

Arab, T., Raffo-Romero, A., van Camp, C., Lemaire, Q., le Marrec-Croq, F., Drago, F., Aboulouard, S., Slomianny, C., Lacoste, A. S., Guigon, I., Touzet, H., Salzet, M., Fournier, I., Lefebvre, C., Vizioli, J., & Sautière, P. E. (2019). Proteomic characterisation of leech microglia extracellular vesicles (EVs): comparison between differential ultracentrifugation and Optiprep™ density gradient isolation. *Journal of Extracellular Vesicles*, *8*(1), 1603048. https://doi.org/10.1080/20013078.2019.1603048

Bekku, Y., Rauch, U., Ninomiya, Y., & Oohashi, T. (2009). Brevican distinctively assembles extracellular components at the large diameter nodes of Ranvier in the CNS. *Journal of Neurochemistry*, *108*(5), 1266–1276. https://doi.org/10.1111/j.1471-4159.2009.05873.x

Bekku, Y., Vargová, L., Goto, Y., Vorísek, I., Dmytrenko, L., Narasaki, M., Ohtsuka, A., Fässler, R., Ninomiya, Y., Syková, E., & Oohashi, T. (2010). Bral1: Its role in diffusion barrier formation and conduction velocity in the CNS. *Journal of Neuroscience*, *30*(8), 3113–3123. https://doi.org/10.1523/JNEUROSCI.5598-09.2010

Bennett, M. L., Bennett, F. C., Liddelow, S. A., Ajami, B., Zamanian, J. L., Fernhoff, N. B., Mulinyawe, S. B., Bohlen, C. J., Adil, A., Tucker, A., Weissman, I. L., Chang, E. F., Li, G., Grant, G. A., Hayden Gephart, M. G., & Barres, B. A. (2016). New tools for studying microglia in the mouse and human CNS. *Proceedings of the National Academy of Sciences of the United States of America*, *113*(12), E1738–E1746. https://doi.org/10.1073/pnas.1525528113

Calabrese, L., Serani, A., Natale, S., Tedeschi, V., Guida, N., Valsecchi, V., Secondo, A., Formisano, L., Annunziato, L., & Molinaro, P. (2022). Identification and characterization of the promoter and transcription factors regulating the expression of cerebral sodium/calcium exchanger 2 (NCX2) gene. *Cell Calcium*, *102*. https://doi.org/10.1016/j.ceca.2022.102542

Cao, Z., Wu, Y., Liu, G., Jiang, Y., Wang, X., Wang, Z., Zhang, J., & Feng, T. (2019). α-Synuclein in salivary extracellular vesicles as a potential biomarker of Parkinson's disease. *Neuroscience Letters*, *696*, 114–120. https://doi.org/10.1016/j.neulet.2018.12.030

Cocozza, F., Grisard, E., Martin-Jaular, L., Mathieu, M., & Théry, C. (2020). SnapShot: Extracellular Vesicles. *Cell*, *182*(1), 262-262.e1. https://doi.org/10.1016/j.cell.2020.04.054

Coleman, B. M., & Hill, A. F. (2015). Extracellular vesicles - Their role in the packaging and spread of misfolded proteins associated with neurodegenerative diseases. In *Seminars in Cell and Developmental Biology* (Vol. 40, pp. 89–96). Academic Press. https://doi.org/10.1016/j.semcdb.2015.02.007

436   Danzer, K. M., Kranich, L. R., Ruf, W. P., Cagsal-Getkin, O., Winslow, A. R., Zhu, L., Vanderburg, C. R., &
437   McLean, P. J. (2012). Exosomal cell-to-cell transmission of alpha synuclein oligomers. *Molecular*
438   *Neurodegeneration*, *7*(1), 1–18. https://doi.org/10.1186/1750-1326-7-42

439   de Lau, L. M., & Breteler, M. M. (2006). Epidemiology of Parkinson's disease. In *Lancet Neurology* (Vol. 5,
440   Issue 6, pp. 525–535). https://doi.org/10.1016/S1474-4422(06)70471-9

441   Dutta, S., Hornung, S., Kruayatidee, A., Maina, K. N., del Rosario, I., Paul, K. C., Wong, D. Y., Duarte Folle,
442   A., Markovic, D., Palma, J. A., Serrano, G. E., Adler, C. H., Perlman, S. L., Poon, W. W., Kang, U. J.,
443   Alcalay, R. N., Sklerov, M., Gylys, K. H., Kaufmann, H., … Bitan, G. (2021). α-Synuclein in blood
444   exosomes immunoprecipitated using neuronal and oligodendroglial markers distinguishes
445   Parkinson's disease from multiple system atrophy. *Acta Neuropathologica*, *142*(3), 495–511.
446   https://doi.org/10.1007/s00401-021-02324-0

447   Eitan, E., Hutchison, E. R., Marosi, K., Comotto, J., Mustapic, M., Nigam, S. M., Suire, C., Maharana, C.,
448   Jicha, G. A., Liu, D., Machairaki, V., Witwer, K. W., Kapogiannis, D., & Mattson, M. P. (2016).
449   Extracellular vesicle-associated aβ mediates trans-neuronal bioenergetic and ca2+-handling deficits
450   in alzheimer's disease models. *Npj Aging and Mechanisms of Disease*, *2*(1).
451   https://doi.org/10.1038/npjamd.2016.19

452   Emmanouilidou, E., Melachroinou, K., Roumeliotis, T., Garbis, S. D., Ntzouni, M., Margaritis, L. H.,
453   Stefanis, L., & Vekrellis, K. (2010). Cell-produced α-synuclein is secreted in a calcium-dependent
454   manner by exosomes and impacts neuronal survival. *Journal of Neuroscience*, *30*(20), 6838–6851.
455   https://doi.org/10.1523/JNEUROSCI.5699-09.2010

456   Fan, R. Z., Guo, M., Luo, S., Cui, M., & Tieu, K. (2019). Exosome release and neuropathology induced by
457   α-synuclein: New insights into protective mechanisms of Drp1 inhibition. *Acta Neuropathologica*
458   *Communications*, *7*(1). https://doi.org/10.1186/s40478-019-0821-4

459   Fearnley, J. M., & Lees, A. J. (1991). Ageing and parkinson's disease: Substantia nigra regional selectivity.
460   *Brain*, *114*(5), 2283–2301. https://doi.org/10.1093/brain/114.5.2283

461   Gámez-Valero, A., Beyer, K., & Borràs, F. E. (2019). Extracellular vesicles, new actors in the search for
462   biomarkers of dementias. In *Neurobiology of Aging* (Vol. 74, pp. 15–20). Elsevier Inc.
463   https://doi.org/10.1016/j.neurobiolaging.2018.10.006

464   Gandhi, S., Wood-Kaczmar, A., Yao, Z., Plun-Favreau, H., Deas, E., Klupsch, K., Downward, J., Latchman,
465   D. S., Tabrizi, S. J., Wood, N. W., Duchen, M. R., & Abramov, A. Y. (2009). PINK1-Associated
466   Parkinson's Disease Is Caused by Neuronal Vulnerability to Calcium-Induced Cell Death. *Molecular*
467   *Cell*, *33*(5), 627–638. https://doi.org/10.1016/j.molcel.2009.02.013

468   George, S., Rey, N. L., Tyson, T., Esquibel, C., Meyerdirk, L., Schulz, E., Pierce, S., Burmeister, A. R., Madaj,
469   Z., Steiner, J. A., Escobar Galvis, M. L., Brundin, L., & Brundin, P. (2019). Microglia affect α-synuclein
470   cell-to-cell transfer in a mouse model of Parkinson's disease. *Molecular Neurodegeneration*, *14*(1),
471   1–22. https://doi.org/10.1186/s13024-019-0335-3

472   Gomes, D. E., & Witwer, K. W. (2022). L1CAM-associated extracellular vesicles: A systematic review of
473   nomenclature, sources, separation, and characterization. *Journal of Extracellular Biology*, *1*(3), e35.
474   https://doi.org/10.1002/jex2.35

475   Gutwein, P., Mechtersheimer, S., Riedle, S., Stoeck, A., Gast, D., Joumaa, S., Zentgraf, H., Fogel, M., &
476   Altevogt, D. P. (2003). ADAM10-mediated cleavage of L1 adhesion molecule at the cell surface and
477   in released membrane vesicles. *The FASEB Journal : Official Publication of the Federation of*
478   *American Societies for Experimental Biology*, *17*(2), 292–294. https://doi.org/10.1096/fj.02-0430fje

479   Gutwein, P., Stoeck, A., Riedle, S., Gast, D., Runz, S., Condon, T. P., Marmé, A., Phong, M. C., Linderkamp,
480   O., Skorokhod, A., & Altevogt, P. (2005). Cleavage of L1 in exosomes and apoptotic membrane
481   vesicles released from ovarian carcinoma cells. *Clinical Cancer Research*, *11*(7), 2492–2501.
482   https://doi.org/10.1158/1078-0432.CCR-04-1688

483   Herbrich, S. M., Cole, R. N., West, K. P., Schulze, K., Yager, J. D., Groopman, J. D., Christian, P., Wu, L.,
484   O'Meally, R. N., May, D. H., McIntosh, M. W., & Ruczinski, I. (2013). Statistical inference from
485   multiple iTRAQ experiments without using common reference standards. *Journal of Proteome*
486   *Research*, *12*(2), 594–604. https://doi.org/10.1021/PR300624G

487   Hijaz, B. A., & Volpicelli-Daley, L. A. (2020). Initiation and propagation of α-synuclein aggregation in the
488   nervous system. In *Molecular Neurodegeneration* (Vol. 15, Issue 1). BioMed Central Ltd.
489   https://doi.org/10.1186/s13024-020-00368-6

490   Hong, Z., Shi, M., Chung, K. A., Quinn, J. F., Peskind, E. R., Galasko, D., Jankovic, J., Zabetian, C. P.,
491   Leverenz, J. B., Baird, G., Montine, T. J., Hancock, A. M., Hwang, H., Pan, C., Bradner, J., Kang, U. J.,
492   Jensen, P. H., & Zhang, J. (2010). DJ-1 and α-synuclein in human cerebrospinal fluid as biomarkers
493   of Parkinson's disease. *Brain*, *133*(3), 713–726. https://doi.org/10.1093/brain/awq008

494   Huang, Y., Cheng, L., Turchinovich, A., Mahairaki, V., Troncoso, J. C., Pletniková, O., Haughey, N. J., Vella,
495   L. J., Hill, A. F., Zheng, L., & Witwer, K. W. (2020). Influence of species and processing parameters
496   on recovery and content of brain tissue-derived extracellular vesicles.
497   *Https://Doi.Org/10.1080/20013078.2020.1785746*, *9*(1).
498   https://doi.org/10.1080/20013078.2020.1785746

499   Hughes, A. J., Daniel, S. E., Ben-Shlomo, Y., & Lees, A. J. (2002). The accuracy of diagnosis of parkinsonian
500   syndromes in a specialist movement disorder service. *Brain*, *125*(4), 861–870.
501   https://doi.org/10.1093/brain/awf080

502   Hu, S., Musante, L., Tataruch, D., Xu, X., Kretz, O., Henry, M., Meleady, P., Luo, H., Zou, H., Jiang, Y., &
503   Holthofer, H. (2018). Purification and Identification of Membrane Proteins from Urinary
504   Extracellular Vesicles using Triton X-114 Phase Partitioning. *Journal of Proteome Research*, *17*(1),
505   86–96. https://doi.org/10.1021/ACS.JPROTEOME.7B00386

506   Jeon, D., Chu, K., Jung, K. H., Kim, M., Yoon, B. W., Lee, C. J., Oh, U., & Shin, H. S. (2008). Na+/Ca2+
507   exchanger 2 is neuroprotective by exporting Ca2+ during a transient focal cerebral ischemia in the
508   mouse. *Cell Calcium*, *43*(5), 482–491. https://doi.org/10.1016/j.ceca.2007.08.003

509   Jeon, D., Yang, Y. M., Jeong, M. J., Philipson, K. D., Rhim, H., & Shin, H. S. (2003). Enhanced learning and
510   memory in mice lacking Na+/Ca2+ exchanger 2. *Neuron*, *38*(6), 965–976.
511   https://doi.org/10.1016/S0896-6273(03)00334-9

512   Jiang, C., Hopfner, F., Berg, D., Hu, M. T., Pilotto, A., Borroni, B., Davis, J. J., & Tofaris, G. K. (2021).
513   Validation of α-Synuclein in L1CAM-Immunocaptured Exosomes as a Biomarker for the

Stratification of Parkinsonian Syndromes. *Movement Disorders*, *36*(11), 2663–2669. https://doi.org/10.1002/mds.28591

Joutsa, J., Gardberg, M., Röyttä, M., & Kaasinen, V. (2014). Diagnostic accuracy of parkinsonism syndromes by general neurologists. *Parkinsonism and Related Disorders*, *20*(8), 840–844. https://doi.org/10.1016/j.parkreldis.2014.04.019

Krämer-Albers, E. M., & Hill, A. F. (2016). Extracellular vesicles: interneural shuttles of complex messages. In *Current Opinion in Neurobiology* (Vol. 39, pp. 101–107). Elsevier Ltd. https://doi.org/10.1016/j.conb.2016.04.016

Li, J. Y., Englund, E., Holton, J. L., Soulet, D., Hagell, P., Lees, A. J., Lashley, T., Quinn, N. P., Rehncrona, S., Björklund, A., Widner, H., Revesz, T., Lindvall, O., & Brundin, P. (2008). Lewy bodies in grafted neurons in subjects with Parkinson's disease suggest host-to-graft disease propagation. *Nature Medicine*, *14*(5), 501–503. https://doi.org/10.1038/nm1746

Li, Q., & Barres, B. A. (2018). Microglia and macrophages in brain homeostasis and disease. In *Nature Reviews Immunology* (Vol. 18, Issue 4, pp. 225–242). Nat Rev Immunol. https://doi.org/10.1038/nri.2017.125

Liu, Y., Zhou, Q., Tang, M., Fu, N., Shao, W., Zhang, S., Yin, Y., Zeng, R., Wang, X., Hu, G., & Zhou, J. (2015). Upregulation of alphaB-crystallin expression in the substantia nigra of patients with Parkinson's disease. *Neurobiology of Aging*, *36*(4), 1686–1691. https://doi.org/10.1016/j.neurobiolaging.2015.01.015

Maas, S. L. N., Breakefield, X. O., & Weaver, A. M. (2017). Extracellular Vesicles: Unique Intercellular Delivery Vehicles. In *Trends in Cell Biology* (Vol. 27, Issue 3, pp. 172–188). Elsevier Ltd. https://doi.org/10.1016/j.tcb.2016.11.003

Mark Frasier and Un Jung Kang. (2014). Parkinson's Disease Biomarkers: Resources for Discovery and Validation. In *Neuropsychopharmacology* (Vol. 39, Issue 1, p. 241). https://doi.org/10.1038/npp.2013.245

McKiernan, J., Noerholm, M., Tadigotla, V., Kumar, S., Torkler, P., Sant, G., Alter, J., Donovan, M. J., & Skog, J. (2020). A urine-based Exosomal gene expression test stratifies risk of high-grade prostate Cancer in men with prior negative prostate biopsy undergoing repeat biopsy. *BMC Urology*, *20*(1), 1–6. https://doi.org/10.1186/s12894-020-00712-4

Norman, M., Ter-Ovanesyan, D., Trieu, W., Lazarovits, R., Kowal, E. J. K., Lee, J. H., Chen-Plotkin, A. S., Regev, A., Church, G. M., & Walt, D. R. (2021). L1CAM is not associated with extracellular vesicles in human cerebrospinal fluid or plasma. *Nature Methods*, *18*(6), 631–634. https://doi.org/10.1038/s41592-021-01174-8

Russell, A. E., Sneider, A., Witwer, K. W., Bergese, P., Bhattacharyya, S. N., Cocks, A., Cocucci, E., Erdbrügger, U., Falcon-Perez, J. M., Freeman, D. W., Gallagher, T. M., Hu, S., Huang, Y., Jay, S. M., Kano, S. ichi, Lavieu, G., Leszczynska, A., Llorente, A. M., Lu, Q., … Vader, P. (2019). Biological membranes in EV biogenesis, stability, uptake, and cargo transfer: an ISEV position paper arising from the ISEV membranes and EVs workshop. *Journal of Extracellular Vesicles*, *8*(1). https://doi.org/10.1080/20013078.2019.1684862

553 Shi, M., Liu, C., Cook, T. J., Bullock, K. M., Zhao, Y., Ginghina, C., Li, Y., Aro, P., Dator, R., He, C., Hipp, M.
554   J., Zabetian, C. P., Peskind, E. R., Hu, S. C., Quinn, J. F., Galasko, D. R., Banks, W. A., & Zhang, J.
555   (2014). Plasma exosomal α-synuclein is likely CNS-derived and increased in Parkinson's disease.
556   *Acta Neuropathologica*, *128*(5), 639–650. https://doi.org/10.1007/s00401-014-1314-y

557 Sokolow, S., Luu, S. H., Headley, A. J., Hanson, A. Y., Kim, T., Miller, C. A., Vinters, H. V., & Gylys, K. H.
558   (2011). High levels of synaptosomal Na+-Ca2+ exchangers (NCX1, NCX2, NCX3) co-localized with
559   amyloid-beta in human cerebral cortex affected by Alzheimer's disease. *Cell Calcium*, *49*(4), 208–
560   216. https://doi.org/10.1016/j.ceca.2010.12.008

561 Stuendl, A., Kraus, T., Chatterjee, M., Zapke, B., Sadowski, B., Moebius, W., Hobert, M. A., Deuschle, C.,
562   Brockmann, K., Maetzler, W., Mollenhauer, B., & Schneider, A. (2021). α-Synuclein in Plasma-
563   Derived Extracellular Vesicles Is a Potential Biomarker of Parkinson's Disease. *Movement Disorders*,
564   *36*(11), 2508–2518. https://doi.org/10.1002/mds.28639

565 Teeple, E., Joshi, P., Pande, R., Huang, Y., Karambe, A., Latta-Mahieu, M., Sardi, S. P., Cedazo-Minguez,
566   A., Klinger, K. W., Flores-Morales, A., Madden, S. L., Rajpal, D., & Kumar, D. (2021). Single Nuclei
567   Sequencing of Human Putamen Oligodendrocytes Reveals Altered Heterogeneity and Disease-
568   Associated Changes in Parkinson's Disease and Multiple System Atrophy. *BioRxiv*,
569   2021.05.06.442967. https://doi.org/10.1101/2021.05.06.442967

570 Théry, C., Witwer, K. W., Aikawa, E., Alcaraz, M. J., Anderson, J. D., Andriantsitohaina, R., Antoniou, A.,
571   Arab, T., Archer, F., Atkin-Smith, G. K., Ayre, D. C., Bach, J.-M., Bachurski, D., Baharvand, H., Balaj,
572   L., Baldacchino, S., Bauer, N. N., Baxter, A. A., Bebawy, M., … Zuba-Surma, E. K. (2019). Minimal
573   information for studies of extracellular vesicles 2018 (MISEV2018): a position statement of the
574   International Society for Extracellular Vesicles and update of the MISEV2014 guidelines. *Journal of
575   Extracellular Vesicles*, *8*(1), 1535750. https://doi.org/10.1080/20013078.2018.1535750

576 Trotta, T., Panaro, M. A., Cianciulli, A., Mori, G., di Benedetto, A., & Porro, C. (2018). Microglia-derived
577   extracellular vesicles in Alzheimer's Disease: A double-edged sword. In *Biochemical Pharmacology*
578   (Vol. 148, pp. 184–192). https://doi.org/10.1016/j.bcp.2017.12.020

579 van Niel, G., D'Angelo, G., & Raposo, G. (2018). Shedding light on the cell biology of extracellular
580   vesicles. *Nature Reviews Molecular Cell Biology*, *19*(4), 213–228.
581   https://doi.org/10.1038/nrm.2017.125

582 Vella, L. J., Scicluna, B. J., Cheng, L., Bawden, E. G., Masters, C. L., Ang, C. S., Willamson, N., McLean, C.,
583   Barnham, K. J., & Hill, A. F. (2017). A rigorous method to enrich for exosomes from brain tissue.
584   *Journal of Extracellular Vesicles*, *6*(1). https://doi.org/10.1080/20013078.2017.1348885

585 Wang, Q., Zhou, Q., Zhang, S., Shao, W., Yin, Y., Li, Y., Hou, J., Zhang, X., Guo, Y., Wang, X., Gu, X., &
586   Zhou, J. (2016). Elevated Hapln2 expression contributes to protein aggregation and
587   neurodegeneration in an animal model of Parkinson's disease. *Frontiers in Aging Neuroscience*,
588   *8*(AUG). https://doi.org/10.3389/fnagi.2016.00197

589 Wood-Kaczmar, A., Deas, E., Wood, N. W., & Abramov, A. Y. (2013). The role of the mitochondrial NCX in
590   the mechanism of neurodegeneration in Parkinson's disease. *Advances in Experimental Medicine
591   and Biology*, *961*, 241–249. https://doi.org/10.1007/978-1-4614-4756-6_20

592   Wood-Kaczmar, A., Gandhi, S., Yao, Z., Abramov, A. S. Y., Miljan, E. A., Keen, G., Stanyer, L., Hargreaves,
593   I., Klupsch, K., Deas, E., Downward, J., Mansfield, L., Jat, P., Taylor, J., Heales, S., Duchen, M. R.,
594   Latchman, D., Tabrizi, S. J., & Wood, N. W. (2008). PINK1 is necessary for long term survival and
595   mitochondrial function in human dopaminergic neurons. *PLoS ONE*, *3*(6), e2455.
596   https://doi.org/10.1371/journal.pone.0002455

597   Wu, X., Zheng, T., & Zhang, B. (2017). Exosomes in Parkinson's Disease. In *Neuroscience Bulletin* (Vol. 33,
598   Issue 3, pp. 331–338). Science Press. https://doi.org/10.1007/s12264-016-0092-z

599   Yáñez-Mó, M., Siljander, P. R. M., Andreu, Z., Zavec, A. B., Borràs, F. E., Buzas, E. I., Buzas, K., Casal, E.,
600   Cappello, F., Carvalho, J., Colás, E., Cordeiro-Da Silva, A., Fais, S., Falcon-Perez, J. M., Ghobrial, I. M.,
601   Giebel, B., Gimona, M., Graner, M., Gursel, I., … de Wever, O. (2015). Biological properties of
602   extracellular vesicles and their physiological functions. In *Journal of Extracellular Vesicles* (Vol. 4,
603   Issue 2015, pp. 1–60). https://doi.org/10.3402/jev.v4.27066

604   Yates, A. G., Pink, R. C., Erdbrügger, U., Siljander, P. R. M., Dellar, E. R., Pantazi, P., Akbar, N., Cooke, W.
605   R., Vatish, M., Dias-Neto, E., Anthony, D. C., & Couch, Y. (2022). In sickness and in health: The
606   functional role of extracellular vesicles in physiology and pathology in vivo: Part I: Health and
607   Normal Physiology. In *Journal of Extracellular Vesicles* (Vol. 11, Issue 1). J Extracell Vesicles.
608   https://doi.org/10.1002/jev2.12151

609   Zhang, Y., Chen, K., Sloan, S. A., Bennett, M. L., Scholze, A. R., O'Keeffe, S., Phatnani, H. P., Guarnieri, P.,
610   Caneda, C., Ruderisch, N., Deng, S., Liddelow, S. A., Zhang, C., Daneman, R., Maniatis, T., Barres, B.
611   A., & Wu, J. Q. (2014). An RNA-sequencing transcriptome and splicing database of glia, neurons,
612   and vascular cells of the cerebral cortex. *Journal of Neuroscience*, *34*(36), 11929–11947.
613   https://doi.org/10.1523/JNEUROSCI.1860-14.2014

614

615
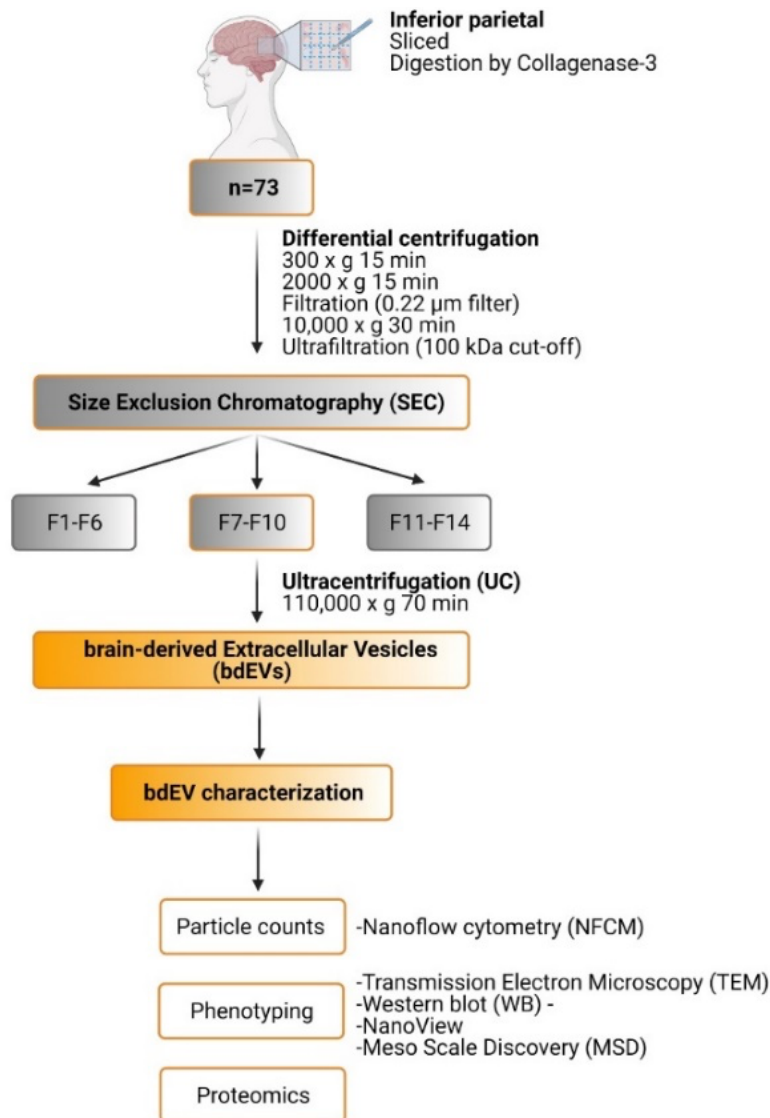
616

617 # Fig. 1

618

619 Figure 1. bdEV separation and characterization workflow. Inferior parietal tissues from 73 human

620 subjects were sliced into small pieces and gently digested. The resulting bdEVs were assessed

621 for particle counts and size distribution using nanoFCM. Further characterizations were done with

622 electron microscopy, Western blot, Single Particle Interferometric Reflectance Imaging Sensor

623 (SP-IRIS), multiplexed ELISA (Meso Scale Discovery), and proteomics. Figure created with
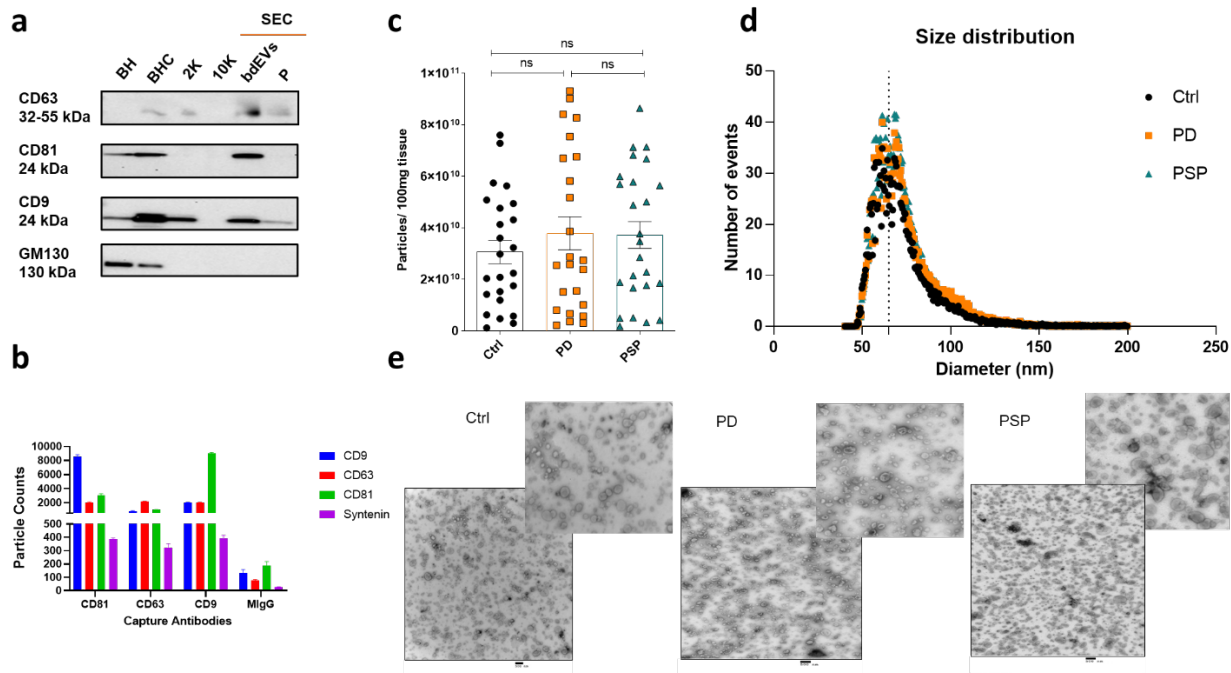
624 BioRender.

625

Fig. 2

Figure 2. bdEV characterization. (a) Western blots of EV surface markers CD63, CD81, and CD9, and Golgi protein GM130 (BH = brain homogenate, BHC = brain homogenate plus collagenase, 2K and 10K = centrifugation pellets, SEC = size exclusion chromatography, with EV fractions and protein (P) fractions. (b). SP-IRIS (fluorescence) detection of tetraspanins (CD9, CD63, CD81) and cytosolic syntenin. Results are presented as mean +/- SD of three capture spots as indicated (CD81, CD63, CD9, and IgG negative control). (c) Particle concentration of human bdEVs by NFCM for control (black), PD (orange), and PSP (green) normalized by tissue input. Data are presented as mean +/- SD. ns: no significant difference (P>0.05), Kruskal-Wallis ANOVA test. (d) Diameter distribution profile (NFCM). (e) Transmission electron micrographs (TEM, scale bar = 500 nm).
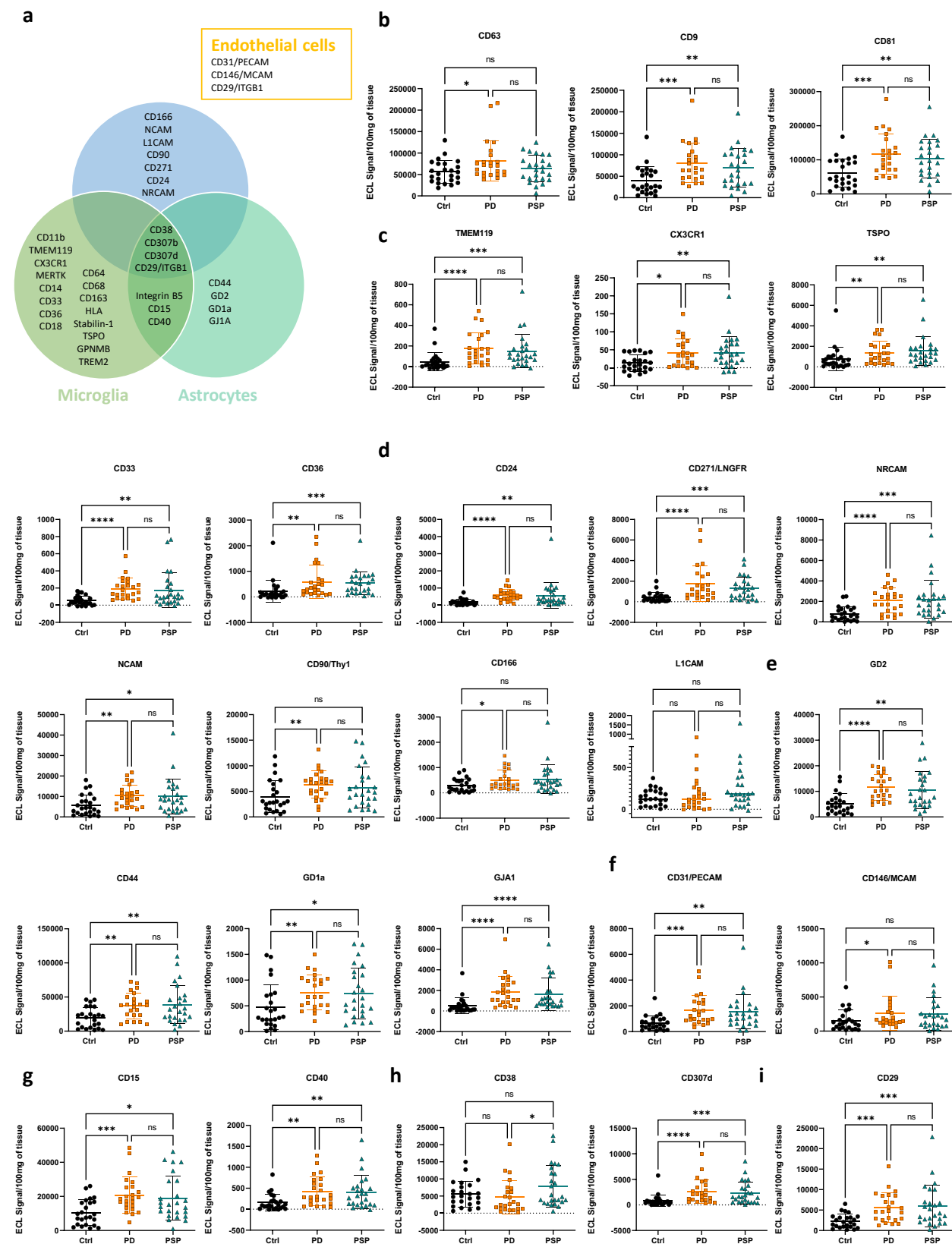
Fig. 3

641   **Figure 3. bdEV phenotyping by multiplexed ELISA.** (a) Distribution of markers by cell type:

642   microglia, neurons, astrocytes, and endothelial cells. Comparison of control (Ctrl), PD, and PSP

643   groups for (b) general markers of EVs and markers of cell of origin: (c) microglia, (d) neurons, (e)

644   astrocytes, (f) endothelial cells; and (g, h, i) markers of multiple populations as indicated. Data

645   were normalized per 100 mg of tissue input and reported as mean +/- SD. Ctrl (n=24); PD (n=24);

646   PSP (n=25). * = $p < 0.05$, ** = $p < 0.01$, *** = $p < 0.001$, **** = $p < 0.0001$, and ns = non-significant

647   (Kruskal-Wallis ANOVA).

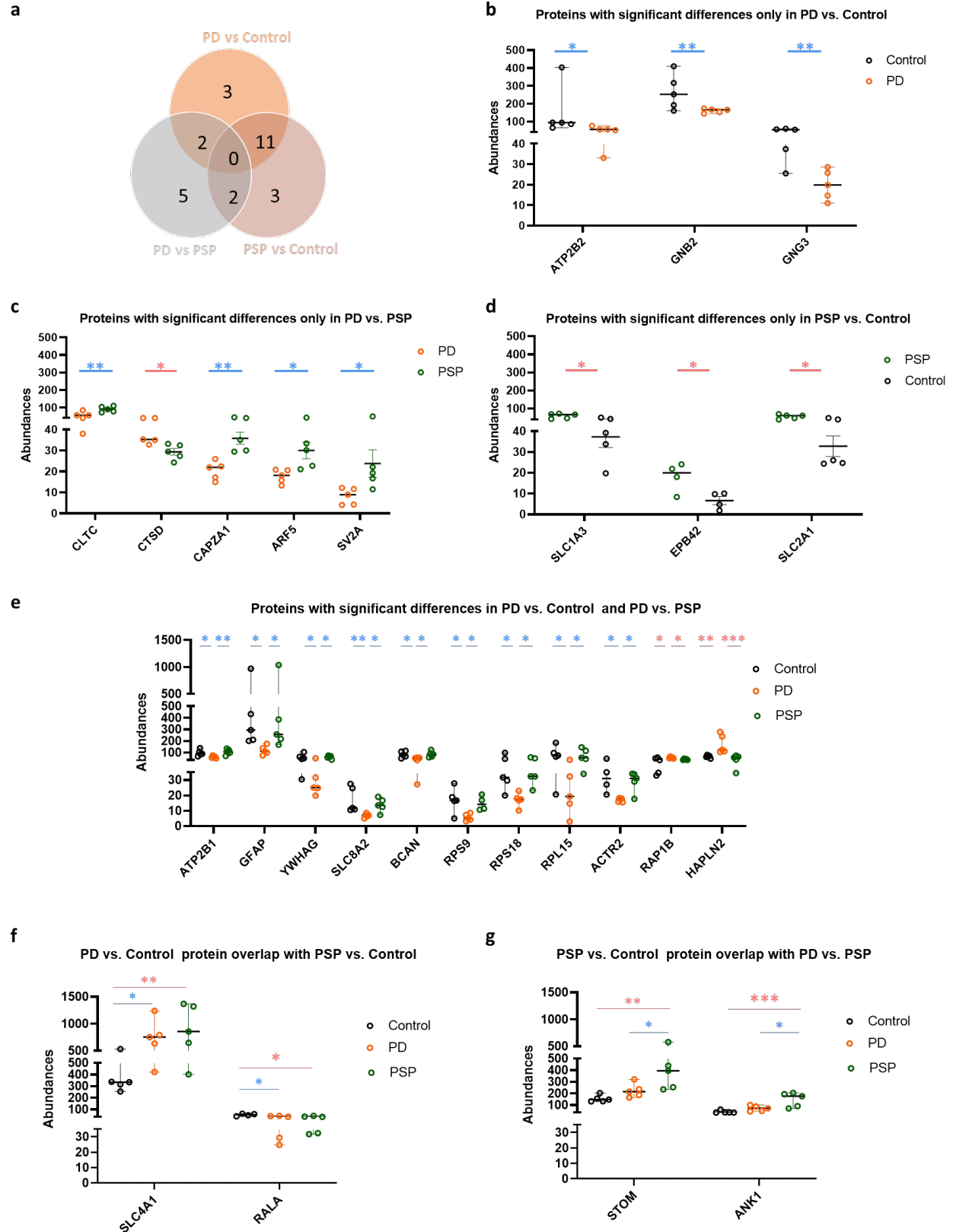## Fig. 4

650 **Figure 4**. **Differential proteomic cargo in bdEVs**. (a) Venn diagram of the number of proteins

651 identified as differentially abundant in multi-group comparison ($p < 0.05$ and log2 fold change >

652 0.32). Protein abundance was normalized by total identified peptides. (b-g) Normalized

653 abundance in multi-group comparisons as indicated. Data are presented as mean +/- SD in

654 control, PD, and PSP. * = $p < 0.05$, ** = $p < 0.01$, *** = $p < 0.001$ following ANOVA. Light blue

655 bars: considered significantly less abundant. Light red bars: considered significantly more

656 abundant.

657

658 ## Table 1. Reagents

Antibodies	Manufacturer	Cat #	Dilution
Primary Anti-CD81	Santa Cruz, Dallas, TX	sc-7637	1:500
Primary Anti-CD63	BD Pharmigen, San Diego, CA	556019	1:1000
Primary Anti-CD9	BioLegend, San Diego, CA	312102	1:1000
Primary Anti-GM130	AbCam, Cambridge, MA	ab52649	1:400
Secondary Mouse Anti-Rabbit IgG BP-HRP	Santa Cruz, Dallas, TX	sc-2357	1:5000
Secondary Rabbit Anti-Mouse IgGk BP-HRP	Santa Cruz, Dallas, TX	516102	1:5000
Primary Anti-TMEM119	Proteintech	27585-1-AP	1:1000
Primary Anti-L1CAM	Biolegend	371602	1:1000

Reagents	Manufacturer	Cat #
100K MWCO Centricon Plus-15	Millipore Sigma	UFC700308
Blotting Grade Blocker	Bio-Rad	170-6404
Carbon Coated 400 Mesh Copper Grids	Electron Microscopy Science	CF400-Cu-UL
Criterion TGX Stain-Free Precast Gel	Bio-Rad	5678084
Distilled Water	Gibco	15230-162
Immuno-Blot PVDF Membrane	Bio-Rad	1620177
Open-Top Thin Wall Ultra-Clear Tubes	Beckman Coulter	344091
Phosphate-Buffered Saline (PBS)	Gibco	14190-144
Polypropylene Ultracentrifugation (UC) Tubes	Sorvall	03-141
RIPA	Cell Signaling Technology	9806
Pierce™ ECL Western Blotting Substrate	Thermo Scientific	32106
Swinging Bucket Rotor AH-629	Thermo Scientific	54284
Tris Buffered Saline (TBS)	Bio-Rad	1706435
Tween-20	Millipore Sigma	P7949

Ultra-Pure Distilled Water	Invitrogen	10977015
Uranyl Acetate	Polysciences	2144725
collagenase 3	Worthington	#CLS-3, S8P18814
Hibernate-E	Thermo Fisher	A1247601
PhosSTOP inhibitor	Sigma-Aldrich	4906837001
Complete Protease Inhibitor	Sigma-Aldrich	11697498001
0.22 um filters	Millipore Sigma	SLGS033SS
Trizol	Thermo Fisher	15596018
Lysing Matrix D beads	MP Biomedicals	116913100

659

Table 2. Subject and tissue information

	PD (n=24)	PSP (n=25)	Control (n=24)	p-value
Age (mean)	79.4 +/- 7.7	76.1 +/- 6.8	77.0 +/- 9.	0.36
Sex (male, female)	9 F/ 15 M	10 F/ 15 M	10 F / 13 M	
PMI, mean (hours)	11.9 +/- 5.8	11.8 +/- 8.0	10.7 +/- 6.0	0.79
Brain tissue weight (mg)	416.86 +/- 78	487.00 +/- 127.27	460.05 +/- 96.28	0.052

Table 3. Differentially abundant proteins

Gene Symbol	PD/C		PSP/C		PD / PSP	
	Abundance Ratio	Abundance Ratio p-value	Abundance Ratio	Abundance Ratio p-value	Abundance Ratio	Abundance Ratio p-value
HAPLN2	1.89	0.004	0.88	0.592	2.16	0.001
SLC8A2	0.6	0.009	1.13	0.739	0.53	0.034
GNG3	0.37	0.009	0.71	0.582	0.53	0.055
ACTR2	0.57	0.012	1.01	0.865	0.57	0.021
RPS9	0.31	0.016	0.83	0.992	0.37	0.028
RALA	0.69	0.024	0.66	0.041	1.04	0.94
GNB2	0.66	0.025	0.81	0.471	0.81	0.194
ATP2B1	0.68	0.026	1.19	0.774	0.57	0.008
BCAN	0.65	0.027	1.05	0.994	0.61	0.022
RPS18	0.55	0.027	1.02	0.992	0.54	0.033
GFAP	0.38	0.028	0.87	0.984	0.43	0.038
SLC4A1	2.25	0.033	2.56	0.012	0.88	0.843
RAP1B	1.58	0.035	1.18	0.996	1.34	0.04
RPL15	0.26	0.036	0.73	0.995	0.35	0.043
YWHAG	0.49	0.043	1.28	0.908	0.38	0.02
ATP2B2	0.6	0.048	0.72	0.191	0.82	0.696
ARF5	0.65	0.069	1.08	0.971	0.6	0.046
EPB42	1.9	0.088	2.92	0.038	0.65	0.785
CAPZA1	0.82	0.105	1.31	0.127	0.63	0.002
ANK1	1.93	0.11	4.72	0.001	0.41	0.032
SLC1A3	1.36	0.116	1.7	0.027	0.8	0.689
SLC2A1	1.94	0.134	2.37	0.026	0.82	0.624
SV2A	0.54	0.139	1.17	0.901	0.46	0.052
STOM	1.46	0.145	2.68	0.001	0.54	0.042
CLTC	0.75	0.169	1.22	0.222	0.62	0.008
CTSD	1.05	0.501	0.87	0.308	1.2	0.048

Light blue: considered significantly less abundant

Light red: considered significantly more abundant

667 ## Table 4: Proteins detected by mass spectrometry and ELISA

Gene name	Protein name	bdEV	PD/C		PSP/C		PD / PSP	
			Abundance Ratio	Abundance Ratio p-Value	Abundance Ratio	Abundance Ratio p-Value	Abundance Ratio	Abundance Ratio p-Value
CD81	CD81 antigen	+	NA	NA	NA	NA	NA	NA
CD44	CD44 antigen	+*	1.08	0.66	1.21	0.24	0.90	0.70
GJA1	gap junction alpha-1 protein	+*	0.89	0.99	1.12	0.95	0.80	0.98
HLA	major histocompatibility complex, class I, B precursor	+*	0.87	0.94	0.91	0.96	0.96	1.00
HLA	HLA class I histocompatibility antigen, C alpha chain precursor	+*	0.85	0.83	1.08	0.99	0.79	0.87
NCAM1	neural cell adhesion molecule 1	+*	0.77	0.44	0.78	0.48	0.99	1.00

668

669   + Detected

670   +* Detected and TMT labeled

671   NA: not applicable

672 Table 5: Proteins identified in bdEVs and in the "Top 100" lists of
673 ExoCarta and/or Vesiclepedia
674

Gene name	Protein name	bdEVs
Overlap between ExoCarta and Vesiclepedia		
A2M	Alpha-2-macroglobulin, Alpha-2-M	-
ACLY	ATP-citrate synthase	-
ACTB	Actin, cytoplasmic 1	+*
ACTN4	Alpha-actinin-4	-
AHCY	Adenosylhomocysteinase	-
ALB	Serum albumin	+*
ALDOA	Fructose-bisphosphate aldolase A	+*
ANXA1	Annexin A1	+*
ANXA11	Annexin A11	+*
ANXA2	Annexin A2	+*
ANXA5	Annexin A5	+*
ANXA6	Annexin A6	+*
ATP1A1	Sodium/potassium-transporting ATPase subunit alpha-1	+*
BSG	Basigin	+*
CCT2	T-complex protein 1 subunit beta	-
CCT3	T-complex protein 1 subunit gamma	-
CD63	CD63 antigen	-
CD81	CD81 antigen	+
CD9	CD9 antigen	-
CDC42	CDC42 small effector protein 1	-
CFL1	Cofilin-1	-
CLIC1	Chloride intracellular channel protein 1	-
CLTC	Clathrin heavy chain 1	+*
EEF1A1	Elongation factor 1-alpha 1	-
EEF2	Elongation factor 2	-
ENO1	Alpha-enolase	+*
EZR	Ezrin	+
FASN	Fatty acid synthase	-
FLNA	Filamin-A	+
FLOT1	Flotillin-1	+
GAPDH	Glyceraldehyde-3-phosphate dehydrogenase	+*
GDI2	Rab GDP dissociation inhibitor beta	-
GNAI2	Guanine nucleotide-binding protein G(i) subunit alpha-2	+*
GNAS	Guanine nucleotide-binding protein G(s) subunit alpha isoforms short	-
GNB1	Guanine nucleotide-binding protein G(I)/G(S)/G(T) subunit beta-1	-
GNB2	Guanine nucleotide-binding protein	+*
HIST1H4A	Histone H4	-

35

HIST1H4B	Histone H4	-
HSP90AA1	Heat shock protein HSP 90-alpha	+*
HSP90AB1	Heat shock protein HSP 90-beta	+
HSPA5	Endoplasmic reticulum chaperone BiP	-
HSPA8	Heat shock cognate 71 kDa protein	+*
ITGB1	Integrin beta-1	-
KPNB1	Importin subunit beta-1	-
LDHA	L-lactate dehydrogenase A chain, LDH-A	+*
LDHB	L-lactate dehydrogenase B chain	-
LGALS3BP	Galectin-3-binding protein	-
MSN	Moesin	+*
MYH9	Myosin-9	+*
PDCD6IP	Programmed cell death 6-interacting protein	-
PFN1	Profilin-1	-
PGK1	Phosphoglycerate kinase 1	+*
PKM	Pyruvate kinase PKM	+*
PPIA	Peptidyl-prolyl cis-trans isomerase A	+*
PRDX1	Peroxiredoxin-1	+*
PRDX2	Peroxiredoxin-2	-
RAB5C	Ras-related protein Rab-5C	+
RAB7A	Ras-related protein Rab-7a	-
RAC1	Ras-related C3 botulinum toxin substrate 1	+*
RAN	GTP-binding nuclear protein Ran	-
RAP1B	Ras-related protein Rap-1b	+*
RHOA	Transforming protein RhoA	+
SDCBP	Syntenin-2	-
SLC3A2	4F2 cell-surface antigen heavy chain, 4F2hc	+*
TCP1	T-complex protein 1	-
TFRC	Transferrin receptor protein 1	-
TPI1	Triosephosphate isomerase	+*
TSG101	Tumor susceptibility gene 101 protein	-
UBA1	Ubiquitin-like modifier-activating enzyme 1	-
VCP	Transitional endoplasmic reticulum ATPase	+*
YWHAB	14-3-3 protein beta/alpha	-
YWHAE	14-3-3 protein epsilon	+*
YWHAG	14-3-3 protein gamma	+*
YWHAQ	14-3-3 protein theta	+*
YWHAZ	14-3-3 protein zeta/delta	+*
Reported in ExoCarta only		
ARF1	ADP-ribosylation factor GTPase-activating protein 1	-
MVP	Major vault protein	+*
RAB1A	Ras-related protein Rab-1A	+
SLC16A1	Monocarboxylate transporter 1	+*
STOM	Erythrocyte band 7 integral membrane protein	-

TKT	Transketolase	+
TUBA1C	Tubulin alpha-1C chain	+*
YWHAH	14-3-3 protein eta	+
Reported in Vesiclepedia only		
ACTN1	alpha-actinin-1	+
ANXA7	annexin A7	+*
C3	complement C3 preproprotein	+
KRT1	keratin, type II cytoskeletal 1	+*
RAB10	ras-related protein Rab-10	+*
RALA	ras-related protein Ral-A	+*

675

676   - Not detected

677   + Detected

678   +* Detected and TMT labeled

679 # Supp Fig. 1

680 a

681

682
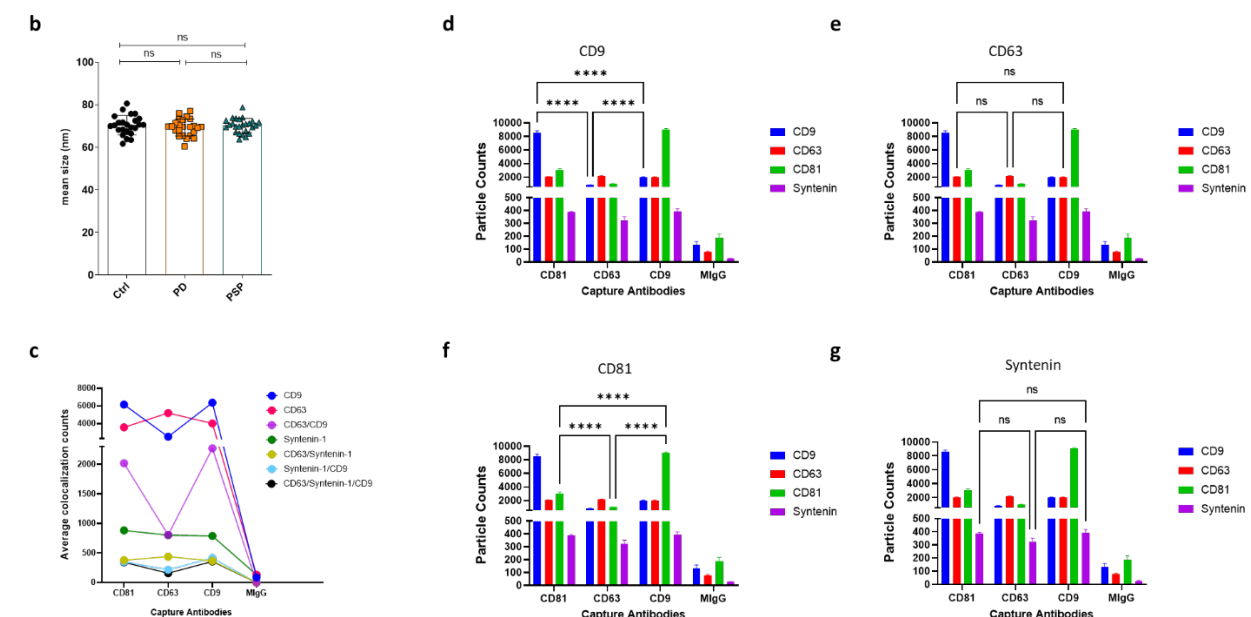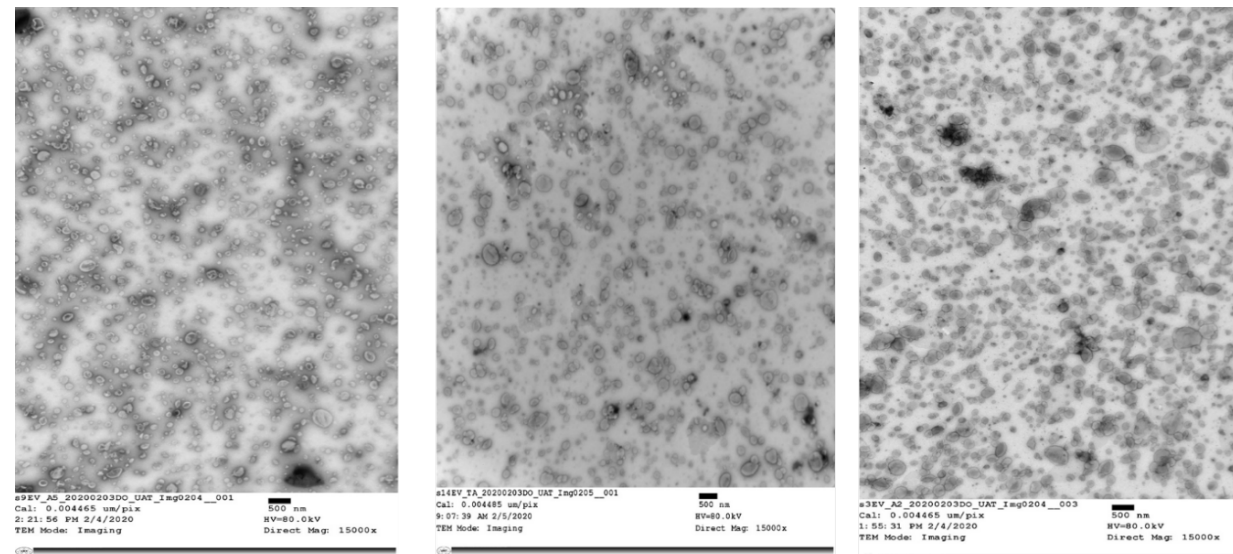
683 **Supp Fig 1. Minimal characterization of bdEVs** (a) Representative transmission electron

684 micrographs (TEM. scale bar = 500 nm). (b) Mean diameter of human bdEVs as measured by

685 nano-flow cytometry (NFCM) for control (black), PD (orange), and PSP (green) and normalized

686 by tissue input. Data are presented as mean +/- SD. ns: no significant difference (P>0.05),

687 Kruskal-Wallis ANOVA test. (c) Mean colocalization counts by SP-IRIS for each capture antibody

688 for single fluorescently-labeled antibodies or combinations, as indicated: CD9, CD63, CD81, and

689   syntenin. In (d-g), statistical analysis is presented for SP-IRIS-detected differences in

690   fluorescence detection of CD9 (d), CD63 (e), CD81 (f), and syntenin (g) associated with each

691   capture antibody, as indicated. Note that the same data are shown in each panel; the multiple

692   panels are to highlight the different comparisons. Results are presented as mean +/- SD. **** = p

693   < 0.0001. and ns = non-significant (two-way ANOVA) of three capture spots as indicated (CD81.
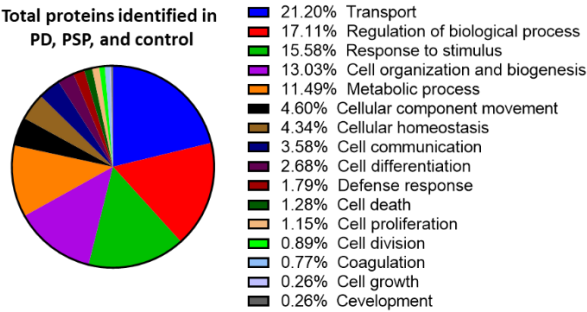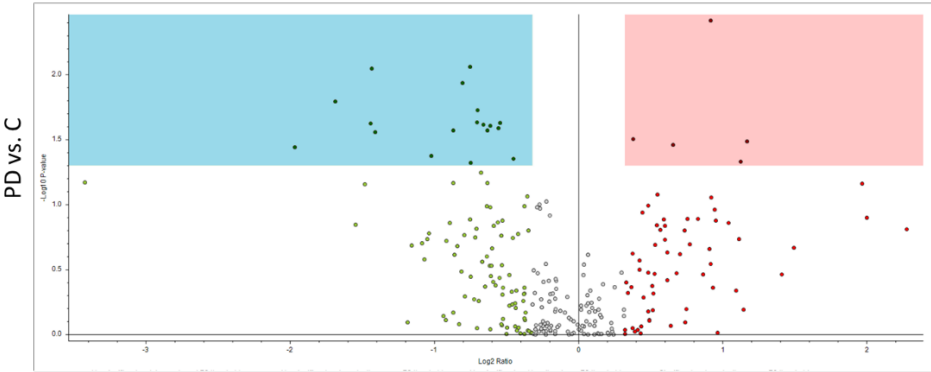
694   CD63, CD9).

Supp Fig. 2
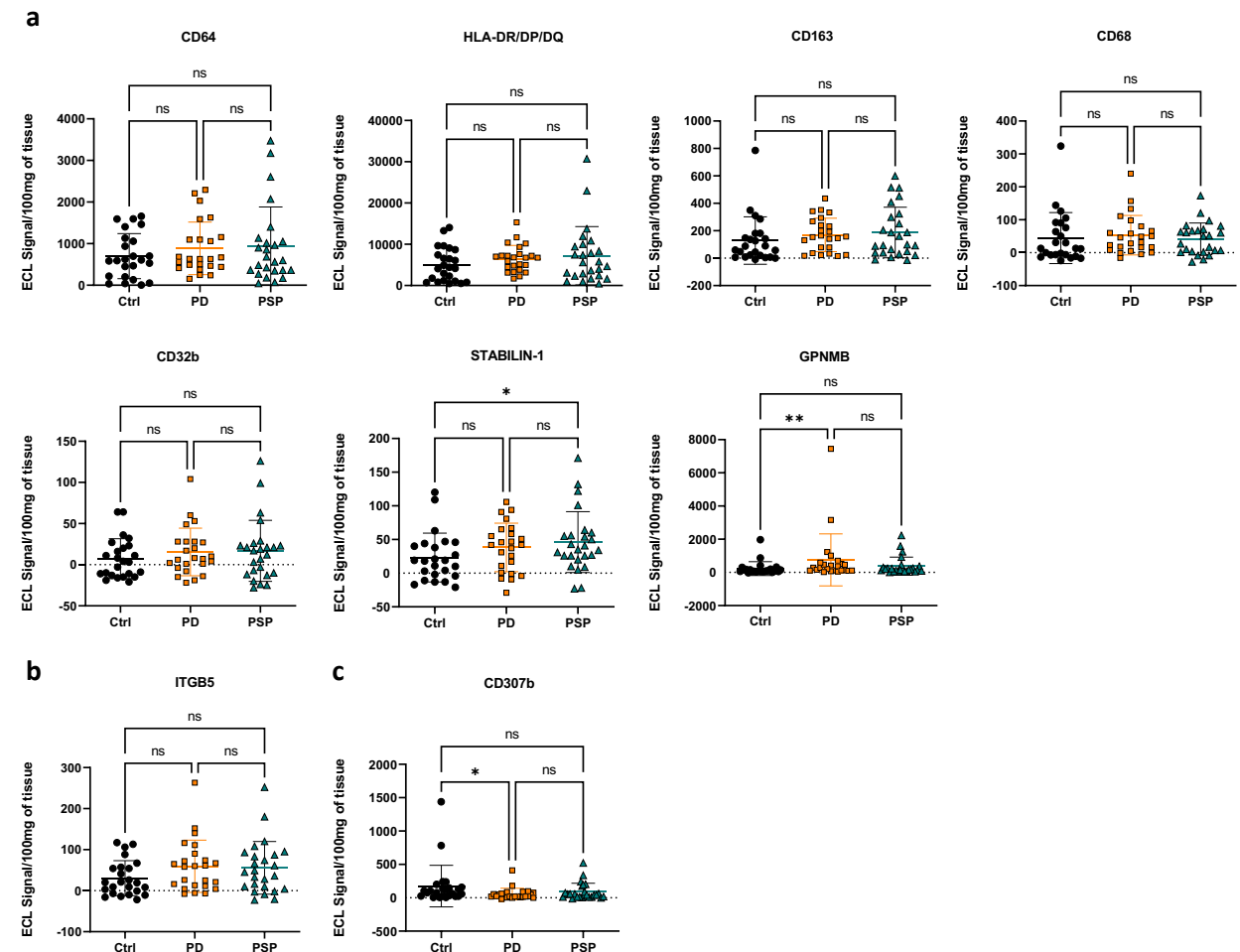
Supp Fig 2. bdEV phenotyping by multiplexed ELISA. Comparison of control (Ctrl), PD, and PSP groups for (a) microglia, (b) microglia and astrocytes, and (c) microglia/neurons/astrocytes (c). Data were normalized per 100 mg of tissue input and reported as mean +/- SD. * = $p < 0.05$. ** = $p < 0.01$. and ns = non-significant (Kruskal-Wallis ANOVA).
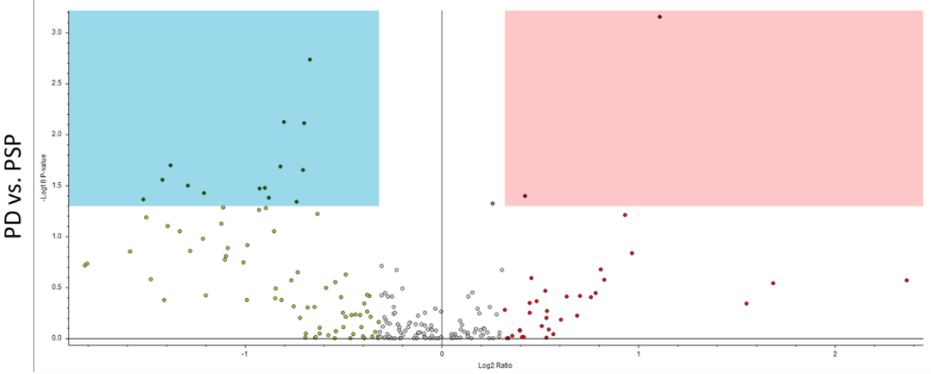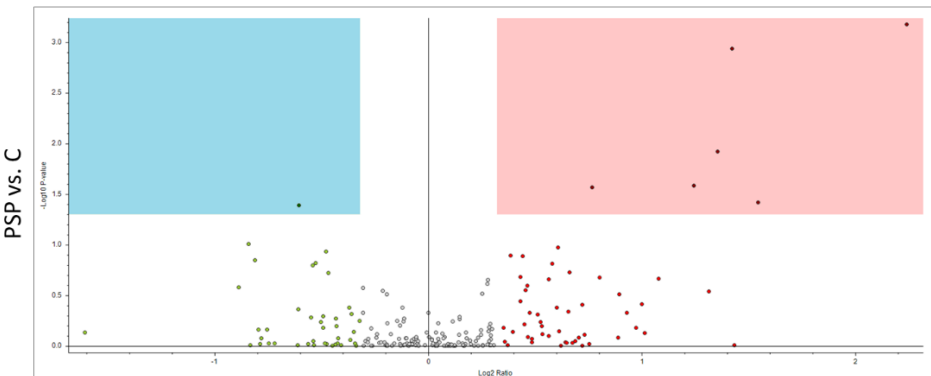
701   # Supp Fig. 3

a

|	
21.20%	Transport
17.11%	Regulation of biological process
15.58%	Response to stimulus
13.03%	Cell organization and biogenesis
11.49%	Metabolic process
4.60%	Cellular component movement
4.34%	Cellular homeostasis
3.58%	Cell communication
2.68%	Cell differentiation
1.79%	Defense response
1.28%	Cell death
1.15%	Cell proliferation
0.89%	Cell division
0.77%	Coagulation
0.26%	Cell growth
0.26%	Cevelopment

b

c

d

702

41

703 **Supp fig. 3: Proteomic profile of bdEVs identified in PD, PSP, and control.** a) Gene Ontology

704 terms associated with the proteome of bdEVs. b-d) Volcano plots of individual proteins of PD vs.

705 control (b), PD vs. PSP (c), and PSP vs. control (d). Light blue squares: considered significantly

706 more abundant. Light red squares: considered significantly less abundant.

707

Supp Fig. 4

a

DisGeNET PD genes   bdEV proteins

1872   80   227

b

709
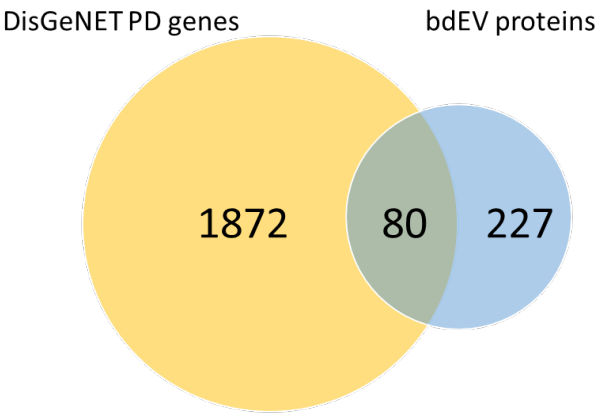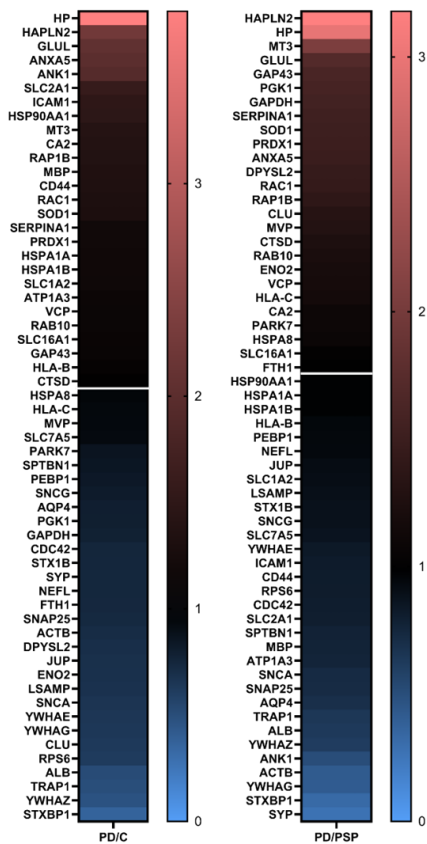
710   **Supp Fig. 4: PD-related proteins and the bdEV proteome.** a) bdEV overlap: PD-related

711   proteins listed in the DisGeNet database and proteins detected in the bdEV proteome and

712   identified in the three tested groups. b) Abundance ratios of individual bdEV proteins from average

713   biological replicates: PD/Control (left) and PD/PSP (right) per the scale shown on the right. White

714   lines correspond to ratio=1.